Structural ordering transition and repulsion of the giant LO-TO splitting in polycrystalline $Ba_xSr_{1-x}TiO_3$

Shou-Yi Kuo, Wen-Yi Liao, and Wen-Feng Hsieh
Institute of Electro-Optical Engineering, National Chiao Tung University, 1001 Tahsueh Rd., Hsinchu 30050, Taiwan
(Received 5 November 2000; revised manuscript received 23 April 2001; published 20 November 2001)

We report Raman and x-ray diffraction studies of polycrystalline $Ba_xSr_{1-x}TiO_3$ (BST) prepared by the sol-gel technique in the range of $x=0$ to 1.0. Other than a tetragonal to cubic phase transition at composition $x\approx0.75$ of the BST powders detected by x-ray diffraction and Raman spectroscopy, a new structural ordering transition around $x\approx0.4-0.5$ is observed due to the atomic arrangement. By taking the anharmonic coupling between the three A_1(TO) modes into account, the observed repulsion of the giant LO-TO splitting is a result of decreasing cell dimension and strengthening the electron-phonon coupling. The results help us to explain the weakening of the ferroelectricity in the BST tetragonal phase as x decreases. The anomalous inconsistency in our experimental results and theoretical prediction are attributed to the lack of detailed information of dynamical effective charges in the $Ba_xSr_{1-x}TiO_3$ compounds.

DOI: 10.1103/PhysRevB.64.224103 PACS number(s): 61.10.Nz

I. INTRODUCTION

Barium strontium titanate ($Ba_xSr_{1-x}TiO_3$, BST) is a dielectric material with excellent dielectric properties such as high dielectric constant, small dielectric loss, low leakage current, and large dielectric breakdown strength. $BaTiO_3$ is a ferroelectric perovskite[1] with Curie temperature T_c at 393 K, while $SrTiO_3$ is a quantum paraelectric[2] whose dielectric constant continues to increase upon cooling down to about 4 K, below which it levels off due to zero-point quantum fluctuations. Thus, it is known that one can control the T_c of BST by adjusting the ratio of Ba/(Ba+Sr) by the approximate relation[3] $T_c(\mathrm{K})=360x+40$, of which a structural change from centrosymmetric cubic to noncentrosymmetric tetragonal phase at room temperature when $x\approx0.75$.

Single crystal $BaTiO_3$ is known to undergo several phase transitions at ambient pressure as a function of temperature using x-ray diffraction, Raman, and infrared spectroscopies.[4–8] The ferroelectric transition occurs as a result of balance between long-range Coulomb interaction and short-range forces. Particularly, the Coulomb interaction can make the ferroelectric instability to details of domain structure, defect and boundary conditions.[9] Another direct effect of such interaction is the splitting of longitudinal optical (LO) and transverse optical (TO) phonons. The calculation of the Born dynamical effective charges, which reflect the local dipole moments developed as atoms being moved, has been performed in ABO_3 cubic perovskite compounds by Zhong *et al.*[9]

Because of the close relationship between ferroelectricity and lattice dynamics, Raman spectroscopy provides a potentially valuable technique for the study of ferroelectric materials. It is highly sensitive to local structure and local symmetry. Compared with other techniques, Raman spectroscopy has two advantages. First, it is a nondestructive method which does not need any special treatment of samples, and second it provides a convenient way of *in situ* observation of changes in the structure with high spatial resolution as a function of temperature, polarization, pressure[10] and electric field.[11] Venkateswaran *et al.*[10] have reported that there are two structural phase transformations through Raman spectra, one at 2 GPa corresponds to the tetragonal to cubic phase transition and the other at 5GPa is still a puzzle. However, the existence of the $BaTiO_3$ Raman spectrum in the paraelectric phase has been reported at high pressure[11] up to 8.6 GPa, and high temperature[6] up to 350 °C. These results had been explained as due to the disorder in the positions of Ti atoms in the polycrystalline samples that breaks the Raman selection rules.

Although there have been a number of Raman and infrared experiments as a function of temperature and pressure on the $BaTiO_3$ since the 1960s,[12–14] there is very little work on the $Ba_xSr_{1-x}TiO_3$ system. In addition, the vibrational properties of $BaTiO_3$ studied by Raman measurements and its temperature dependence of the coupling parameters have been obtained based on the coupled-phonon model. In order to avoid influences of the volume when temperature changed, the composition-dependent experiment of $Ba_xSr_{1-x}TiO_3$ has an advantage over temperature in studying the effect of phase transition on the coupling of the phonon states. Recently, $Ba_xSr_{1-x}TiO_3$ system prepared by solid-state reaction shows the lattice parameter as a function of x closely follows Vegard's law.[3,15] However, the samples prepared by sol-gel technique did not show the same tendency.[16] In this paper, we present the x-ray diffraction (XRD) and Raman study of polycrystalline $Ba_xSr_{1-x}TiO_3$ powders with x varying from 0 to 1. The lattice constants were calculated from XRD $\theta-2\theta$ scans and the detailed Raman studies were analyzed by coupled-phonon model. From the spectra, the characteristics of the tetragonal-to-cubic phase transition and a new observed structural ordering are discussed.

II. EXPERIMENT

In our experiments, the sol-gel technique was employed for preparing $Ba_xSr_{1-x}TiO_3$ polycrystalline powders to yield samples with high composition accuracy and homogeneity.[16] We first boiled acetic acid to 120 °C for producing dehy-

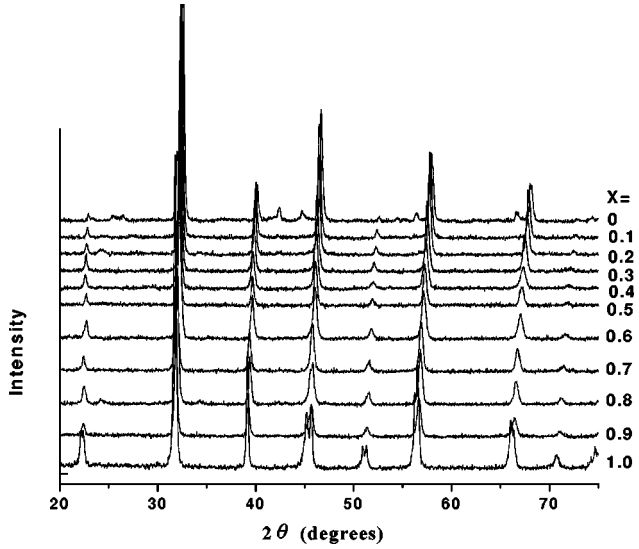

FIG. 1. Powder XRD patterns of $Ba_xSr_{1-x}TiO_3$ samples with various x values.

drated solvent. A proper amount of barium acetate and strontium acetate (99% purity from Gransman Inc.) was dissolved in dehydrated acetic acid at 90 °C and was sufficiently stirred for 20 min. Titanium isopropoxide and some di-ethanol were then added to the solution and were stirred for another 20 min. We dried and solidified the solution by illuminating with a 400 W infrared lamp for two days. The resulting white solid was heated to 165 °C for an hour and then was ground into powders. We then sintered the powders at 1000 °C for 150 min in an Al_2O_3 boat. This sintering temperature is far below the melting point of any composition of BST which is required for the conventional solid-state reaction.

X-ray powder diffraction patterns were obtained using SHIMADZU XD-5 diffractometer and monochromated high intensity Cu-$\kappa\alpha$ line of wavelength 1.5405 Å over the range $20° \leqslant 2\theta \leqslant 75°$ by using with both step-scanning mode of integration time 1 sec with 0.01 degree per step and a continuous 2θ scan of 4°/min. The patterns were then Gaussian fitted to get the diffraction peaks and widths. We obtain basically the same results from different scanning modes. Thus, we only show the patterns of continuous scan mode in the following section. For Raman measurement, the 488 nm line of an Ar^+ laser, which is far from resonance with band-gap energy of $Ba_xSr_{1-x}TiO_3$, was used as the excitation source. The scattered light was analyzed using a SPEX 1877C triple spectrograph equipped with a cooled CCD (PHOTOMETRICS CC200) at −90 °C. It is not possible to obtain polarized spectra because there is no preferred orientation of the polycrystalline samples. Thus, all spectra reported in this study are unpolarized from polycrystalline $Ba_xSr_{1-x}TiO_3$.

III. RESULTS AND DISCUSSION

Figure 1 shows x-ray diffraction (XRD) patterns of the samples with various x values obtained by the aforementioned sol-gel processes. The resulting XRD patterns were then analyzed with Rietvelt refinement procedure.[17] In this procedure, we used the tetragonal structure for all BST compounds to obtain the lattice constants of the a axis and c axis. When BST's belong to the tetragonal system, the initial data of (101), (110), (111), (112), (211), (202), and (220) planes together with the JCPDS data are input to the XLAT program[17] (a personal computer program for the refinement of lattice constants), whereas, only one of the degenerate peaks [e.g., (101) and (110) are degenerate] are used for the cubic phases. The results were plotted in Fig. 2 with the statistical residuals being less than 0.1%. The lattice constants of our synthesized $BaTiO_3$ polycrystalline powder agree well with previous literature[18,19]as 4.003 and 3.897 Å for $SrTiO_3$. We found, in Fig. 2(a), both the lattice constants of the a axis and c axis follow the Vegard's law for $0 < x \leqslant 0.4$, but off the Vegard's law for $x > 0.4$ where an obvious discontinuity at $x \approx 0.7$ corresponds to the well-known tetragonal-cubic phase transition. It also can be seen that the ratio of c/a almost equals to 1 when $x \leqslant 0.75$ from Fig. 2(b), then drastically increases from 1 as further increasing x. It further confirms the tetragonal-cubic phase transition around $x \approx 0.7-0.75$. The other turning point around $x \approx 0.4-0.5$ has not been reported for $Ba_xSr_{1-x}TiO_3$. Similar behavior has also been observed in our previous data of the effective

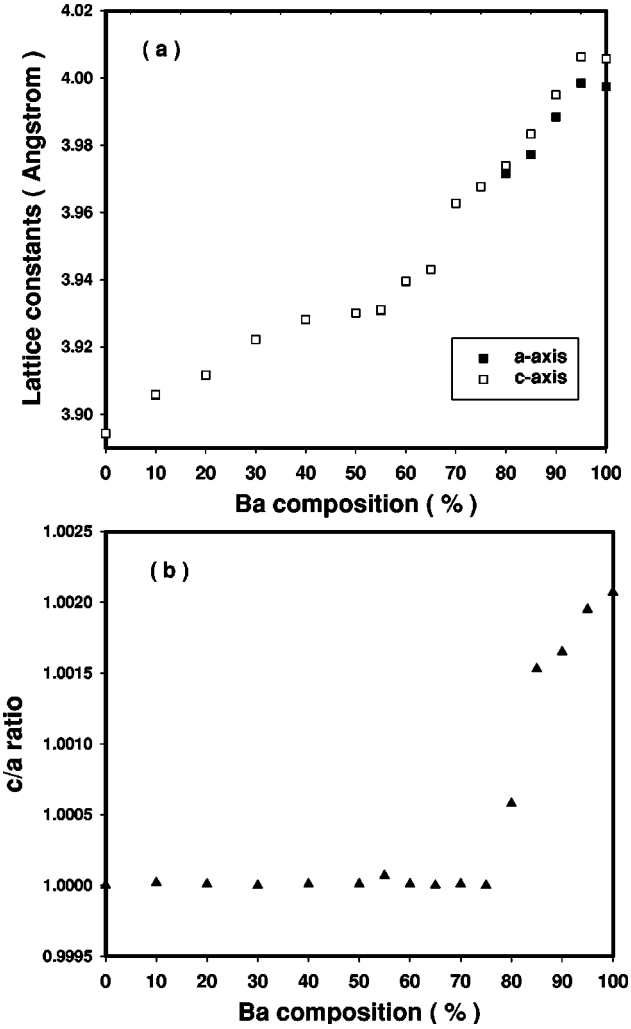

FIG. 2. The lattice constants a and c of $Ba_xSr_{1-x}TiO_3$ after Rietvelt refinement procedure (a) and the ratio of c/a (b).

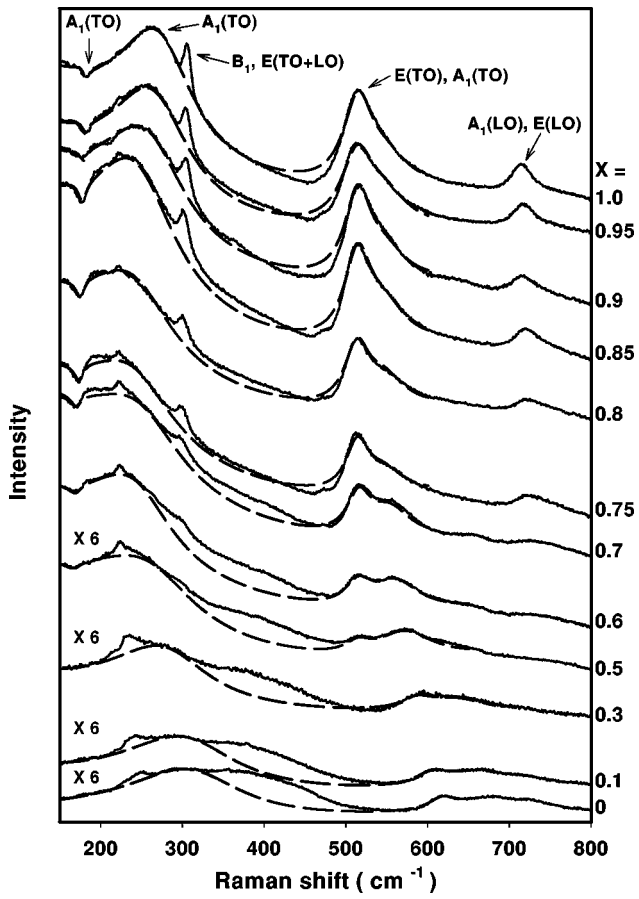

FIG. 3. Unpolarized Raman spectra of polycrystalline $Ba_xSr_{1-x}TiO_3$ [x from 0 to 1 and the dashed line represent the simulated specta $I(\omega)$].

second harmonic generation coefficients and birefringence of these samples,[16] therefore, it is believed this result is not an experimental artifact.

The Raman spectra of $Ba_xSr_{1-x}TiO_3$ polycrystalline powders taken at room temperature are plotted in Fig. 3 for various x values. Furthermore, we have increased the acquisition time of the cubic phase BST by 6 times, labeled in the figure, for $x<0.7$. First of all, we found in pure $BaTiO_3$ powder there is a dip at 180 cm^{-1} which was assigned to $A_1(TO_1)$ phonon mode, a broad band centered at 260 cm^{-1} corresponds to $A_1(TO_2)$ phonon mode, a sharp peak at 305 cm^{-1} is attributed to the B_1 and $E(TO+LO)$ modes, and the asymmetric broad band near 520 cm^{-1} corresponds to $E(TO)$ and $A_1(TO_3)$ modes. Finally, the highest frequency peak near 720 cm^{-1} was observed, in which both $A_1(LO)$ (the hardest LO mode) and $E(LO)$ character seems to be present. In addition to the aforementioned phenomena, the Raman peaks at 305 and 720 cm^{-1} are specific to the tetragonal phase of the $BaTiO_3$ as described in Ref. 6. Our polycrystalline specimens are randomly oriented so do not admit the polarization selection between A_1 and E modes. The observed Raman peaks of the $BaTiO_3$ polycrystalline agree well with the powder Raman spectra reported by Osada *et al.*[8] and with the reported for polycrystalline thin film grown by rf sputtering.[20]

As x decreases from 1 to 0.7, the sharp peak at 310 cm^{-1} does not show evidently frequency shift but weakens and disappears when $x<0.7$. Whereas, the $A_1(LO)/E(TO)$ mode at 720 cm^{-1} monotonously increases in its frequency as varying x from 1 to 0.7 and disappears at $x\approx 0.7$. In addition, the appearance of spectral dip at 180 cm^{-1}, which corresponds to the softest $A_1(TO)$ mode, has been explained as an interference due to the anharmonic coupling between the three $A_1(TO)$ phonons.[11]

In addition to the dip, the broad band near 260 cm^{-1} $[A_1(TO_2)]$ shifts to low frequency for $0.7<x<1$, and then to higher frequency for even lower x. The asymmetric broad band near 500–600 cm^{-1} consisting of an $E(TO)$ mode at 518 cm^{-1} and a $A_1(TO_3)$ mode on the high frequency shoulder[14] has a remarkable change in its lineshape. The observed Raman spectra became noisy when $x<0.7$. It is interesting to note that the $Ba_xSr_{1-x}TiO_3$ undergoes a phase transition from ferroelectric to paraelectric phase when $x\approx 0.7$. The broadened spectra observed in the paraelectric phase indicates that the Raman selection rule is relaxed ascribed to the disorder in the positions of the Ti atoms in the unit cells of the polycrystalline samples.[13,19] The Raman results would show the instantaneous symmetry of our specimens if it is lower than the cubic.

In order to ascertain the influence of the coupling effect, Sood[21] and Chaves *et al.*[22] have considered the anharmonic coupling effect to distinguish three individual phonon modes in earlier Raman studies on $BaTiO_3$, $SrTiO_3$, $AlPO_4$ and a-quartz. The Raman line shape can be expressed as

$$I(\omega)=A[n(\omega)+1]\mathrm{Im}[\mathbf{T^*GT}], \tag{1}$$

where the inverse matrix response is

$$\mathbf{G}^{-1}(\omega)=\mathbf{\Omega}^2-\omega^2\mathbf{I}-i\omega\mathbf{\Gamma}. \tag{2}$$

$[n(\omega)+1]$ is the usual Bose-Einstein factor, A is a constant, and $\mathbf{T}$ is a vector involving Raman scattering amplitudes. In this equation $\mathbf{I}$ is the unit matrix, $\mathbf{\Omega^2}$ the force constant matrix, and $\mathbf{\Gamma}$ the damping matrix are expressed as follows:

$$\mathbf{\Omega}^2=\begin{pmatrix}\omega_1^2 & \omega_{12}^2 & 0\\ \omega_{12}^2 & \omega_2^2 & \omega_{23}^2\\ 0 & \omega_{23}^2 & \omega_3^2\end{pmatrix},\mathbf{\Gamma}=\begin{pmatrix}\Gamma_1^2 & 0 & 0\\ 0 & \Gamma_2^2 & 0\\ 0 & 0 & \Gamma_3^2\end{pmatrix} \tag{3}$$

with ω_i and ω_{ij} $(i,j=1\cdots 3)$ being the frequencies of uncoupled modes and the coupling strength between modes i and j. It has been assumed the coupling between ω_1 and ω_3 is negligible with $\omega_{13}=0$.

Although we observed disappearance of $A_1(TO_1)$ dips and broadening of $A_1(TO_3)$ mode as $x<0.5$ from Fig. 3, in order to fit well with measured spectra, we still used the coupled-phonon model to fit the observed Raman spectra in the whole composition range and obtained the fitting parameters. Using similar simulation procedure described in Ref. 21, we first subtracted the spectra by a second order polynomial which fits to the base line of the spectra and used the elements of $\mathbf{\Gamma}$, $\mathbf{\Omega^2}$, and $\mathbf{T}$ as adjusting parameters of the

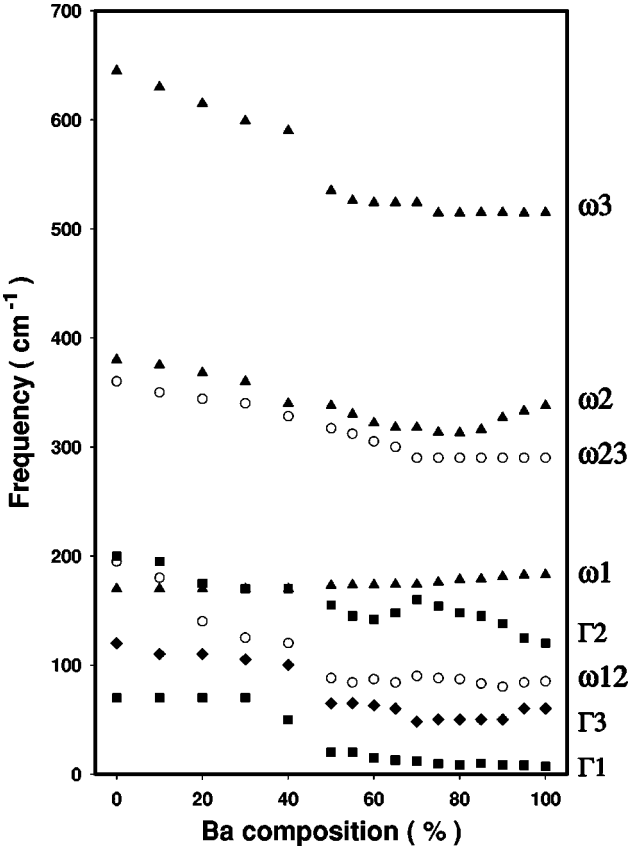

FIG. 4. The fitted parameters plotted as a function of x (Ba composition).

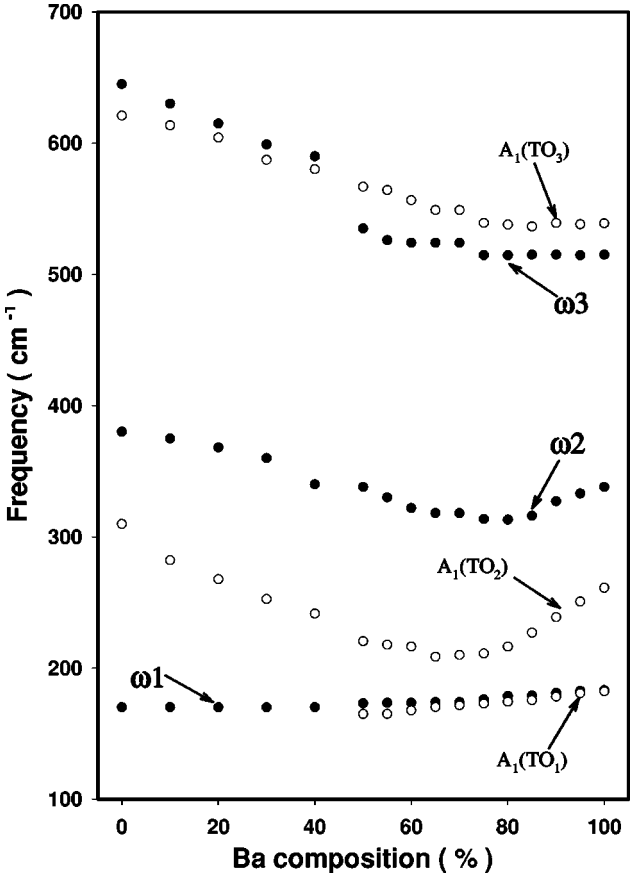

FIG. 5. The as-read peak positions from the data as well as the values obtained from the fit of the data to the coupled-phonon model (drawn by solid symbols) are plotted as a function of x (Ba composition).

calculated $I(\omega)$ to obtain the least squares among 120–330 cm^{-1} and 480–650 cm^{-1} related to the three $A_1(\mathrm{TO})$ and $E(\mathrm{TO})$ modes.

The fitted parameters were plotted in Fig. 4 and came up with the following features when x decreases from 1 to 0. (i) ω_1 continuously soften and ω_3 displays a trend toward the higher value with two discontinuities occurred around x at 0.75 and 0.5. (ii) ω_2 slightly decreases as varying x from 1 to 0.75 and then monotonically increases. (iii) The linewidth Γ_1 and Γ_3 show the similar behavior having distinct discontinuities near $x=0.5$. Moreover, Γ_2 of the $A_1(\mathrm{TO}_2)$ mode reaches a local maximum at $x\approx 0.75$ due to tetragonal to cubic phase transition then increases when $x<0.5$. (iv) The coupling constant ω_{12} is almost constant in the range of $0.5<x<1$ and progressively increases as $x<0.5$. (v) Whereas, ω_{23} is almost 2–3 times larger than ω_{12} and shows a noticeable turning point near $x\approx 0.7$. To sum up the statements above, we found that $x\approx 0.7-0.8$ is the well-known tetragonal to cubic phase transition and a new transition occurs at $x\approx 0.4-0.5$, in which the fitting parameters, e.g., ω_{12}, Γ_1, Γ_2, and Γ_3, show some variation that is consistent with the x-ray diffraction, second-harmonic generation, and birefringence measurements.[16] The severe broadening of the linewidths (or high phonon decaying rates) and decreasing in amplitudes of three $A_1(\mathrm{TO})$ modes reflect the selection rule of Raman cross section that the characteristic of these modes vanish in cubic phase. In addition, we believe that the disappearance and broadening of Raman modes around 518 cm^{-1} $[E(\mathrm{TO})]$ and 180 cm^{-1} are also indicatives of some structural reordering taking place near $x\approx 0.5$.

Figure 5 shows the plot of as-read peak positions from the data as well as the values of three A_1-symmetry TO modes obtained from the coupled-phonon model. It can be seen that the composition-dependent frequency shifts of decoupled ω_1, ω_2 and ω_3 have similar tendency with the as-read ones. However, the stronger coupling ($\omega_{23}>\omega_{12}$) between $A_1(\mathrm{TO}_2)$ and $A_1(\mathrm{TO}_3)$ causes the repulsion of these modes, especially it brings about the $A_1(\mathrm{TO}_2)$ undergoing a minimum around $x\approx 0.7$.

Figure 6 shows the peak of $A_1(\mathrm{LO}_3)$ mode at 720 cm^{-1} and $A_1(\mathrm{TO}_1)$ mode versus Ba composition. It indicates a linear splitting of these two modes in the tetragonal phase. According to the calculation of Born effective charges of ABO_3 perovskites by Zhong *et al.*,[9] we comprehend that the calculated mode effective charge for the softest TO mode is the largest as listed in Table III of Ref. 9. It means that the softest mode will couple most strongly with the electric field. Due to strong mode mixing via Coulomb interaction, the softest TO $[A_1(\mathrm{TO}_1)]$ mode is most closely associated with the hardest LO $[A_1(\mathrm{LO}_3)]$ mode that gives rise to a giant LO-TO splitting in ABO_3 compounds, especially for the ferroelectric phonon modes. From Fig. 1(b), the cell dimension of $\mathrm{Ba}_x\mathrm{Sr}_{1-x}\mathrm{TiO}_3$ decreases when x changes from 1 to

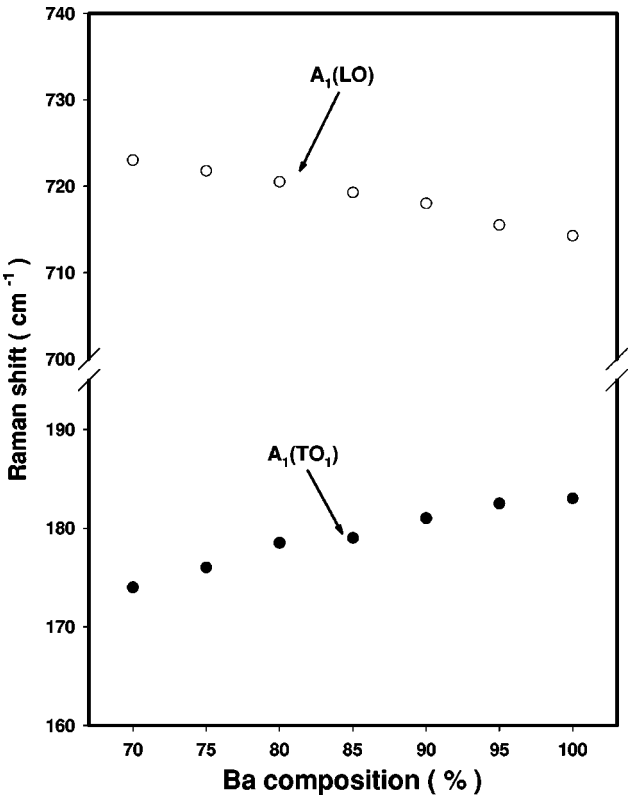

FIG. 6. The LO-TO splitting of the $A_1(\mathrm{LO})$ and $A_1(\mathrm{TO}_1)$ modes for $Ba_xSr_{1-x}TiO_3$ at $x>0.7$.

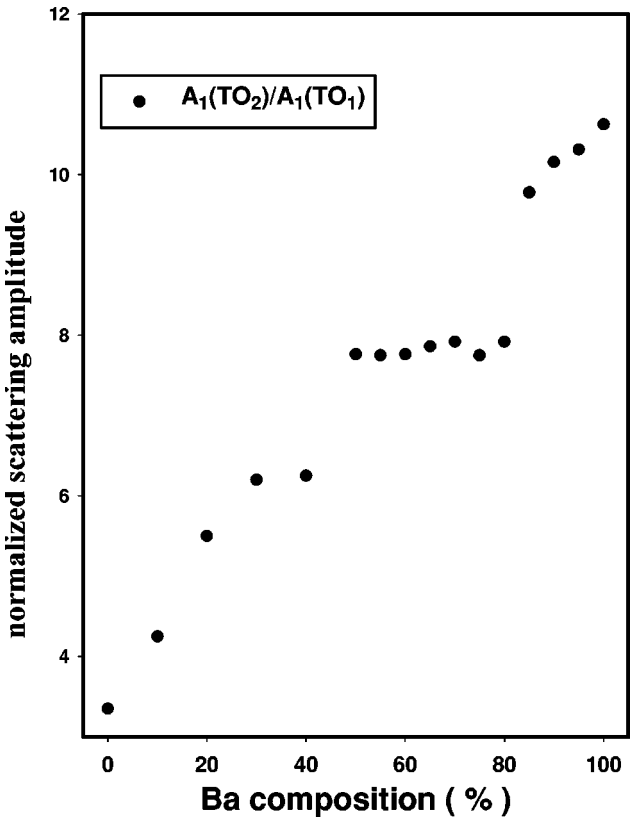

FIG. 7. The normalized scattering amplitudes of $A_1(\mathrm{TO}_2)/A_1(\mathrm{TO}_1)$ as a function of Ba composition.

0.7. The decrease of cell dimension strengthens coupling of the $A_1(\mathrm{TO}_1)$ mode and $A_1(\mathrm{LO}_3)$ mode by

$$D_{mn}^{\mathrm{LO}}=D_{mn}^{\mathrm{TO}}+\frac{4\pi e}{\Omega}\frac{Z_m^*Z_n^*}{\varepsilon_\infty(0)}, \tag{4}$$

where D is the dynamical matrix, Ω the volume of the unit cell, and Z^* the Born effective charge. It has been known that the Coulomb interaction will play a very important role in the occurrence of ferroelectricity.[23] In other words, it was demonstrated that this feature is associated with the existence of an anomalously large destabilizing dipole-dipole interaction, sufficient to compensate the stabilizing short-range forces and induce the ferroelectric instability. Thus, as expected and from our Raman and XRD studies, $Ba_xSr_{1-x}TiO_3$ undergo a transition from tetragonal to cubic phase at $x\approx0.75$. We have verified from Fig. 5 the increase of giant LO-TO splitting as decreasing x will weaken the ferroelectricity as the first-principle calculation by Zhong *et al.*[9] It can be seen that the differences between the LO and TO frequencies denoting the Coulomb interaction arose from the last term in Eq. (4). The variation of the cell dimension Ω [see Figs. 1(a) and Fig. 3 of Ref. 16] in tetragonal phase would lead the LO-TO splitting to become nonlinear which is different from our linear result. The inconsistency may be due to strong coupling between three $A_1(\mathrm{TO})$ modes and lack of detailed information on the dynamical effective charges for $Ba_xSr_{1-x}TiO_3$ compounds.

The normalized scattering amplitudes T_2/T_1 are shown in Fig. 7 as a function of x (Ba mole fraction). It is noted that the tendency is similar to the effective nonlinearities reported by Chen *et al.*[7] Figure 8 shows the projections of $A_1(\mathrm{TO}_1)$ and $A_1(\mathrm{TO}_2)$ vibration modes of perovskite structure. The oxygen atoms and cation oscillate oppositely in the $A_1(\mathrm{TO}_2)$ mode. Unlike the $A_1(\mathrm{TO}_2)$ mode, the TiO_6 octahedron and Ba (Sr) atoms vibrate in opposite directions at TO_1 mode. It is well known that $BaTiO_3$ belongs to the displacement type of ferroelectric material and it is believed that the $Ba_xSr_{1-x}TiO_3$ is of the same type. The spontaneous polarization P_s can be expressed as $P_s=P_0'\cdot\Delta z$, where Δz denotes the displacement of ions from the symmetric positions which are occupied in the paraelectric phase. From the discussion above, we infer that the $A_1(\mathrm{TO}_2)$ mode is more sensitive to the dipole displacement than the $A_1(\mathrm{TO}_1)$ mode. It can be seen from Fig. 7 that the normalized T_2/T_1 lower its values as decreasing x. In the meanwhile, there is a discontinuity occurred near $x\approx0.7-0.8$ and it is closely related to the tetragonal to cubic phase transition.

From the x-ray and Raman measurements on polycrystalline $Ba_xSr_{1-x}TiO_3$ presented in Figs. 1–7, we deduce that there are two structural rearrangements; one between x at 0.7 and 0.8 which corresponds to the well-studied ferroelectric to paraelectric phase transition and the other at x near 0.5 which has not been reported for $Ba_xSr_{1-x}TiO_3$ system. In the paraelectric phase of the BST, the Raman spectra imply that this phase does not have perfect cubic symmetry but has some disorder which break the symmetry and permit Raman activity. The reported results by Naik *et al.* of high-pressure Raman experiments of polycrystalline $BaTiO_3$ has show evi-

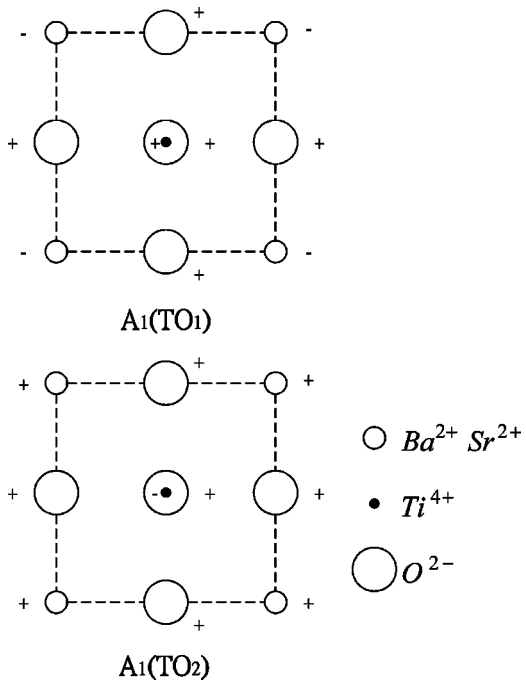

FIG. 8. Projections of $A_1(TO_1)$ and $A_1(TO_2)$ vibration modes of perovskite structure.

dence for a new structural phase transformation near 5 GPa. Further experiments indicated the observed changes in the Raman spectra need not be due to contributions from rhombohedral, orthorhombic and hexagonal phases.

The spontaneous polarization of a ferroelectric crystal had been shown varying with temperature according to[24] $P_s = a\sqrt{T_c - T}$, while the second-order nonlinear optical (NLO) coefficient had been proposed proportional to the spontaneous polarization of a ferroelectric crystal.[25] Since T_c obeys the approximate relationship as[3] T_c (K) $= 360x + 40$ in $Ba_xSr_{1-x}TiO_3$, we expect to observe the NLO coefficient which varies with the mole fraction of Ba by the square-root law as well. However, in the previous study,[16] we observed that the trend of NLO coefficient and birefringence versus x had similar behavior to the cell dimension. The NLO coefficient and birefringence of $Ba_xSr_{1-x}TiO_3$ linearly depend on the cell dimension other than obeying the square-root law. The anomalous discrepancy between the experimental results and prediction of the references 24 and 25 maybe results from the dynamical effective charges[9] should be regarded as composition dependence.

The turning point arround $x \approx 0.4-0.5$ observed in XRD and Raman analyses may be caused by the atomic arrangement during the sample growth procedure. Due to the Ba atom possesses larger radius than Sr, the introduction of Ba to substitute Sr will surely enlarge the lattice denoted in XRD that normally obeys the Vegard's law.[3,15] Let us discuss the lattice change due to Ba atomic substitution starting from the pure $SrTiO_3$ crystal ($x=0$). According to the thermodynamics, the free energy of BST should be minimized when keeping on substituting Sr by Ba, the excess Ba atoms would avoid occupying the nearest-neighbor positions.

Since $SrTiO_3$ crystal belong to cubic structure, it has the basis of

$$\text{Sr:} \quad (0,0,0),$$

$$\text{Ti:} \quad (1/2,1/2,1/2),$$

$$3\ \text{O:} \quad (1/2,1/2,0);\ (1/2,0,1/2);\ (0,1/2,1/2)$$

in a unit cell and with three primary lattice vectors $\vec{a} = (1,0,0)$, $\vec{b} = (0,1,0)$, and $\vec{c} = (0,0,1)$, respectively. Assume the first substituting Ba atom occupies at the coordinate $(0,0,0)$ in a specific unit cell. The coordinates of $(\pm 1, \pm 1, \pm 1)$ are those of isomorphic lattices belonging to the neighboring unit cells; thus, the successive substituting Ba atoms tend to sit at one of the next nearest-neighboring positions in the unit cell to suppress the lattice expansion. Otherwise, the lattice will be dramatically elongated to raise the free energy. While $x = 0.5$, half of the Sr atoms have been replaced by Ba atoms to force Ba to sit next to each other and suddenly increase its lattice constants [see Fig. 2(a)]. The observed turning points in lattice constants along with the phonon frequencies and coupling constants from XRD and Raman spectra is a result of cell distortion around $x = 0.4 \sim 0.5$. Our BST powders are prepared by sol-gel technique at room temperature, and the atom arrangement may have been determined during the gelation. Although the powder samples were sintered at 1000 °C, we believe that the temperature is far below the melting point of BST and will not provide enough free energy for atom rearrangement. The free energy supplied by the thermal energy during sample preparation could lead two Ba atoms to sit next to each other at Ba content around x between 0.4–0.5 rather than at $x = 0.5$ that was illustrated above for zero temperature. On the other hand, the extra thermal energy would have relaxed the lattice to cause atomic rearrangement when the BST powders were synthesized under high temperature by using solid-state reaction method.[3,15] Thus the previous reported XRD and Raman measurements did not show the same consequence.

IV. CONCLUSION

In summary, we have investigated the XRD and Raman spectra of $Ba_xSr_{1-x}TiO_3$ prepared by sol-gel method. The lattice constants of the $Ba_xSr_{1-x}TiO_3$ were estimated from XRD spectra and the phase transition behavior was examined. The analysis of the Raman and XRD spectra under various mole fractions of Ba indicates that there are at least two structural phase transitions. The first one occurring at $x \approx 0.7$ corresponds to the transition from tetragonal to cubic phases. The second transition occurs around $x \approx 0.4-0.5$ which has not been reported in previous studies by solid-state reaction method. We explained that the experimental evidence might be due to the atomic arrangement of samples during sol-gel preparation at lower temperature compared to that prepared by the conventional solid-state reaction method. The coupled-phonon model has been used to determine the composition dependence of mode frequencies, line-

widths, transition amplitudes, and coupling parameters. Since no Raman activity is expected in the cubic phase, the observation of the Raman spectra at the region is attributed to the presence of disorder. The observed repulsion of LO-TO splitting is a result of decreasing cell dimension and strengthening the electron-phonon coupling. The anomalous inconsistency in our experimental results and prediction of Refs. 24, 25, and 9 may be due to lack of detailed information on the dynamical effective charges for $Ba_xSr_{1-x}TiO_3$ compounds. Further molecular dynamical study is underway to determine the mechanism of the observed structural ordering.

[1] H. P. Roaksby and H. D. Megaw, Nature (London) **155**, 484 (1945).
[2] K. A. Muller and H. Burkard, Phys. Rev. B **19**, 3593 (1979).
[3] V. V. Lemanov, Phys. Solid State **39**, 318 (1997).
[4] F. Jona and G. Shirane, *Ferroelectric Crystals* (Pergamon, New York, 1962).
[5] J. A. Sanjurjo, R. S. Katiyar, and S. P. S. Porto, Phys. Rev. B **22**, 2396 (1980).
[6] R. Naik, J. J. Nazarko, C. S. Flattery, U. D. Venkateswaran, V. M. Naik, M. S. Mohammed, G. W. Auner, J. V. Mantese, N. W. Schubring, A. L. Micheli, and A. B. Catalan, Phys. Rev. B **61**, 11 367 (2000).
[7] C. Li, Z. Chen, and H. Lu, J. Appl. Phys. **86**, 4555 (1999).
[8] M. Osada, M. Kakihana, and W. Cho, Appl. Phys. Lett. **75**, 3393 (1999).
[9] W. Zhong, R. D. King-Smith, and D. Vanderbilt, Phys. Rev. Lett. **72**, 3618 (1994).
[10] U. D. Venkateswaran, V. M. Naik, and R. Naik, Phys. Rev. B **58**, 14 256 (1998).
[11] I. A. Akimov, A. A. Sirenko, A. M. Clark, J. H. Hao, and X. X. Xi, Phys. Rev. Lett. **84**, 4625 (2000).
[12] A. Pinczuk, W. Taylor, and E. Burstein, Solid State Commun. **5**, 429 (1967).
[13] J. L. Parsons and L. Rimai, Solid State Commun. **5**, 423 (1967).
[14] M. DiDomenico, S. H. Wemple, and S. P. Porto, Phys. Rev. **174**, 524 (1968).
[15] V. V. Lemanov, E. P. Smirnova, P. P. Syrnikov, and E. A. Tarakanov, Phys. Rev. B **54**, 3151 (1996).
[16] W. K. Chen, C. M. Cheng, J. Y. Huang, and W. F. Hsieh, J. Phys. Chem. Solids **61**, 959 (2000).
[17] A computer program for Rietveld analysis of x-ray and neutron powder diffraction patterns (http://www-structure.llnl.gov).
[18] Y. A. Abramov, V. G. Tsirelson, V. E. Zavodnik, and I. D. Brown, Acta Crystallogr., Sect. B: Struct. Sci. **51**, 942 (1995).
[19] S. A. Howard, J. K. Yau, and H. U. Anderson, J. Appl. Phys. **65**, 1492 (1989).
[20] B. Wang, L. D. Zhang, L. Zhang, Y. Yan, and S. L. Zhang, Thin Solid Films **354**, 262 (1999).
[21] A. K. Sood, N. Chandrabhas, D. V. S. Muthu, and A. Jayaraman, Phys. Rev. B **51**, 8892 (1995).
[22] A. Chaves, R. S. Katiyar, and S. P. S. Porto, Phys. Rev. B **10**, 3522 (1974).
[23] J. D. Axe, Phys. Rev. **157**, 429 (1967).
[24] G. A. Smolensky, J. Phys. Soc. Jpn. **28**, 26 (1970).
[25] F. Wang, Phys. Rev. B **59**, 9733 (1999).